OXFORD

Deep learning assisted quantitative analysis of Aβ and microglia in patients with idiopathic normal pressure hydrocephalus in relation to cognitive outcome

Antti J. Luikku (ID), MD*,[1,2], Ossi Nerg (ID), MD, MSc[3,4], Anne M. Koivisto, MD, PhD[3,4,5,6],
Tuomo Hänninen, PhD[3,4], Antti Junkkari (ID), MD, PhD[2], Susanna Kemppainen, PhD[7],
Sini-Pauliina Juopperi, MSc[7], Rosa Sinisalo, MSc[7], Alli Pesola, BSc[1],
Hilkka Soininen, MD, PhD[4], Mikko Hiltunen, PhD[7], Ville Leinonen, MD, PhD[1,2],
Tuomas Rauramaa, MD, PhD[8,9], Henna Martiskainen, PhD[7]

[1]Institute of Clinical Medicine—Neurosurgery, University of Eastern Finland, Kuopio, Finland
[2]Neurosurgery of NeuroCenter, Kuopio University Hospital, Kuopio, Finland
[3]Neurology of NeuroCenter, Kuopio University Hospital, Kuopio, Finland
[4]Institute of Clinical Medicine—Neurology, University of Eastern Finland, Kuopio, Finland
[5]Department of Neurosciences, University of Helsinki, Helsinki University Hospital, Helsinki, Finland
[6]Department of Geriatrics/Rehabilitation and Internal Medicine, University of Helsinki, Helsinki University Hospital, Helsinki, Finland
[7]Institute of Biomedicine, University of Eastern Finland, Kuopio, Finland
[8]Department of Pathology, Kuopio University Hospital, Kuopio, Finland
[9]Institute of Clinical Medicine—Pathology, University of Eastern Finland, Kuopio, Finland

*Send correspondence to: Antti J. Luikku, MD, Institute of Clinical Medicine—Neurosurgery, University of Eastern Finland, P.O. Box 1627, FI-70211 Kuopio, Finland; E-mail: antti.luikku@kuh.fi

Author contributions: T. Rauramaa and H. Martiskainen contributed equally to this work.

ABSTRACT

Neuropathologic changes of Alzheimer disease (AD) including Aβ accumulation and neuroinflammation are frequently observed in the cerebral cortex of patients with idiopathic normal pressure hydrocephalus (iNPH). We created an automated analysis platform to quantify Aβ load and reactive microglia in the vicinity of Aβ plaques and to evaluate their association with cognitive outcome in cortical biopsies of patients with iNPH obtained at the time of shunting. Aiforia Create deep learning software was used on whole slide images of Iba1/4G8 double immunostained frontal cortical biopsies of 120 shunted iNPH patients to identify Iba1-positive microglia somas and Aβ areas, respectively. Dementia, AD clinical syndrome (ACS), and Clinical Dementia Rating Global score (CDR-GS) were evaluated retrospectively after a median follow-up of 4.4 years. Deep learning artificial intelligence yielded excellent (>95%) precision for tissue, Aβ, and microglia somas. Using an age-adjusted model, higher Aβ coverage predicted the development of dementia, the diagnosis of ACS, and more severe memory impairment by CDR-GS whereas measured microglial densities and Aβ-related microglia did not correlate with cognitive outcome in these patients. Therefore, cognitive outcome seems to be hampered by higher Aβ coverage in cortical biopsies in shunted iNPH patients but is not correlated with densities of surrounding microglia.

KEYWORDS: Alzheimer disease; beta amyloid; brain biopsy; cognition; convoluted neural network; deep learning; dementia; microglia; normal pressure hydrocephalus

INTRODUCTION

Alzheimer disease (AD) is a major neurodegenerative disorder that profoundly impairs cognitive functions.[1] The diagnosis of AD clinical syndrome (ACS) is based on neurological examination as well as neuropsychological profiling supported by progress of symptoms during follow-up, and brain imaging.[1,2] Amyloid-beta (Aβ) plaques and pathologic tau deposits in vivo are the hallmarks of neuropathologically verified AD.[2] Aβ accumulation, a potential target for early diagnosis and treatment modalities, seems to initiate up to 20 years prior to the onset of clinical symptoms.[3,4] In addition to accumulation of Aβ and tau, neuroinflammation by activated microglia and astrocytes has a prominent role in the pathogenesis of AD. Contribution of microglia to AD pathogenesis has been emphasized by the identification of multiple AD risk variants in microglial genes.[5,6] Microglia are

highly dynamic immune cells that constantly survey their environment for perturbations of central nervous system homeostasis such as accumulation of Aβ, which leads to microglial transition towards different activation states and clustering around Aβ plaques.[7–9] Plaque-associated microglia have been proposed to form a protective barrier and restrict the toxicity of Aβ plaques,[10,11] while this barrier function can be hampered by genetic AD risk factors or comorbidities such as diabetes.[9,12–14]

Idiopathic normal pressure hydrocephalus (iNPH) is a degenerative brain disease of so far unknown etiology. INPH impairs gait, urinary incontinence, and cognitive functions in various combinations and has an incidence of 1.8-7.3/ 100 000.[15] The diagnosis of iNPH is based on clinical symptoms, enlarged ventricles in brain imaging and patient history.[16] Despite rigorous research, ventriculomegaly remains as the sole biomarker for the diagnosis of iNPH.[16–18] The majority of NPH patients benefit from shunt surgery and selection can be aided with prognostic tests, such as cerebrospinal fluid (CSF) removal test.[19,20] AD and vascular dementia are the most important clinical differential diagnoses of iNPH.[21,22] Up to 50% of patients with symptoms suggestive of iNPH have also showed AD pathology in the cortical brain biopsies,[17] and over one-fifth of iNPH patients develop clinical AD on follow-up.[23] Thus, frontal cortical biopsies obtained at the time of shunt surgery to treat iNPH offer a unique opportunity to study early AD-related neuropathological changes in living patients.[24]

Traditionally, evaluation of neuropathological changes in histological sections is based on visual assessment and involves semiquantitative scoring or manual counting. Such analyses are laborious and time-consuming, often require specific expertise, and may be prone to inter-observer variation. To overcome these limitations, deep learning-based models such as convolutional neural network (CNN) have recently been implemented to assess different neuropathological changes in whole slide images (WSIs) of stained histological sections.[25,26] The CNN is trained by human-made annotations from desired histopathological features in WSIs, eg, Aβ or microglial cells, and yields data from analyzed images based on the training.[27,28] After initial training and validation, CNN models can quickly produce quantitative data from a large number of histological sections. The models can easily be re-used when new samples or new datasets become available and can be shared between research centers to ensure consistent analysis in multi-center studies.

In this study, we aimed to build a CNN-based AI model for the detection of Aβ-associated microglial cells in human brain tissue using Aiforia Create CNN, which is operated in a commercial cloud-based Aiforia platform[29] and does not require prior knowledge of deep learning. We used the developed CNN models to derive quantified amounts of Aβ, Aβ-associated microglia, and total microglial density in a cohort of 120 shunted iNPH patients, and correlate these measures to the development of major neurodegenerative disorder and the severity of memory impairment by Clinical Dementia Rating Global score (CDR-GS).

METHODS
Patients

Neurosurgery of NeuroCenter in the Kuopio University Hospital (KUH) serves the defined catchment population in Eastern Finland. Since 1993, the diagnostic workup of KUH Neurosurgery for suspected NPH has included a clinical examination by a neurologist and a neurosurgeon, CT or MRI scan of the brain, and a right frontal cortical biopsy.[21,30] In routine evaluations, the cortical biopsies were stained as previously described.[31] Aβ and hyperphosphorylated tau-pathology was assessed semiquantitatively by a neuropathologist (T.R.). Brain biopsies were part of routine clinical care and informed consent was obtained from all patients.

The Kuopio NPH Registry (www.uef.fi/nph) consists of 929 consecutive patients to the end of the year 2017 and includes baseline and follow-up data from KUH, all primary health care physicians, and other local hospitals in the KUH catchment area. Selection criteria for study population were: (1) shunt surgery for iNPH between 9/2010 and the end of the year 2017; (2) positive Aβ in routine neuropathological analysis; and (3) frontal cortex biopsy sample available for further analysis (Figure 1). Positive tau-pathology (AT8) was observed in 23% of the study population samples. Demographic data are shown by development of major neurodegenerative disorder (dementia) in Table 1, by the presence of ACS in Table 2, and by the CDR-GS in Table 3. Patients evaluated for suspected NPH fulfilled the following criteria: (1) 2-3 symptoms related to NPH, ie, impaired cognition, gait, or urinary continence; and (2) enlarged brain ventricles, ie, Evans' index >0.3 in CT or MRI examinations.

Selection for shunt surgery was done with a 3-step protocol: first, a lumbar CSF removal of 20-40 mL (CSF tap test) was
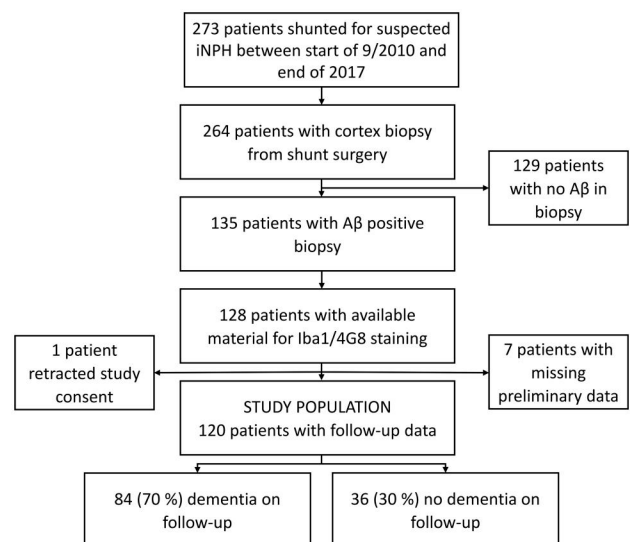

Figure 1. Flowchart of the 273 patients with suspected idiopathic normal pressure hydrocephalus (iNPH) between 9/2010 and the end of 2017 from the Kuopio NPH Registry. The study population consisted of 120 patients shunted for idiopathic NPH with adequate follow-up data and frontal cortical biopsies with Iba1/4G8 staining. Development of dementia (major neurodegenerative disorder) was observed during the follow-up.

performed for all patients, and 20% improvement in gait speed was considered a positive response[30]; patients with a negative tap test underwent a lumbar infusion test, where conductance of 10 or less was considered pathological.[32] Those with negative results both in the tap test and the infusion test were shunted based on expert opinion. Ventriculoperitoneal shunts with an adjustable PS Medical Strata valve were used for shunting. During the ventricular catheter insertion, a cortical sample was obtained with a 2-mm biopsy needle (Temno Evolution 14G). The initial response to the shunt, ie, defined as improvement in the patient's gait, memory, or urinary incontinence, was observed by the clinician 2-3 months after the shunt placement at the outpatient clinic.[21]

The clinical follow-up was continued at local hospitals and by primary care physicians. The study population (Figure 1) was followed for a median period of 4.4 years (range 0.1-10), during which time 58 (48%) of the patients died. Data from KUH archives, local hospitals, primary care physicians, and nursing reports was collected. AD was diagnosed according to revised NINCDS-ADRDA criteria,[33] and examinations by geriatricians and neurologists were considered. For this study, these clinical diagnoses of AD were considered as ACS, as per the NIA-AA Research Framework.[2] Follow-up information of the study population was evaluated (A.M.K., O.N., A.J.L.) to determine CDR-GS[34] (ordinal scale to address severity of memory disease: 0 = healthy, 0.5 = very mild, 1 = mild, 2 = moderate 3 = severe) and major neurodegenerative disorder (dementia).[35]

If shunt malfunction was suspected during the follow-up, the patients were referred for neurological and neurosurgical re-evaluation. A total of 11 patients underwent shunt revision during the follow-up period.

All procedures performed in studies involving human participants were in accordance with the ethical standards of the institutional and/or national research committee and with the 1964 Helsinki declaration and its later amendments or comparable ethical standards.

APOE genotyping

A PCR method was used in the analysis of *APOE*, as described previously.[36] The presence of ε4 allele was scored as either present or absent for the analysis.

Table 1. Demographics of the study population by major neurodegenerative disorder (dementia) at follow-up.

	Dementia $n = 84$	No dementia $n = 36$	P-value[a]
Male/female	39/45	18/18	.842
Age at shunt operation, years	79 (64-88)	76 (62-87)	.003
Follow-up time, years	4.7 (0.13-10)	4.3 (1.4-10)	.984
Preoperative MMSE	20 (4-28)	26 (19-29)	<.001
APOE ε4	44 (52%)	15 (42%)	.323
Initial shunt response	55 (66%)	32 (89%)	.008
Shunt revision during follow-up	5 (6%)	6 (17%)	.084
Deceased during follow-up	42 (50%)	16 (44%)	.691

Abbreviation: MMSE = Mini-Mental State Examination (range 0-30, 30 indicating no deterioration in cognition).
Variables are shown in median (range) or number (%).
^a [a] Fisher exact test with Bonferroni correction was used for categorical variables, Mann–Whitney *U*-test for continuous.

Table 2. Demographics of the study population by Alzheimer disease clinical syndrome (ACS) at follow-up.

	ACS $n = 46$	No ACS $n = 74$	P-value[a]
Male/female	20/26	37/37	.574
Age at shunt operation, years	80 (65-88)	78 (62-88)	.001
Follow-up time, years	4.4 (0.48-9.9)	4.4 (0.13-10)	.983
MMSE	19 (4-27)	24 (6-29)	<.001
APOE ε4	24 (52%)	35 (47%)	.708
Initial shunt response	31 (67%)	56 (76%)	.401
Shunt revision during follow up	1 (2%)	10 (14%)	.049
Deceased during follow-up	25 (54%)	33 (45%)	.349

Abbreviation: MMSE = Mini-Mental State Examination (range 0-30, 30 indicating no deterioration in cognition).
Variables are shown in median (range) or number (%).
[a] Fisher exact test with Bonferroni correction was used for categorical variables, Mann–Whitney *U*-test for continuous.

Table 3. Demographics of the study population by Clinical Dementia Rating Global score at follow-up.

CDR-GS	0 $n = 4$	0.5 $n = 33$	1 $n = 20$	2 $n = 26$	3 $n = 37$	r_s[a]
Male/female	1/3	17/16	8/12	13/13	18/19	.022
Age at shunt operation, years	73 (69-80)	76 (62-87)	78 (64-87)	79 (69-88)	80 (65-88)	.245*
Follow-up time, years	5.0 (4.3-7.2)	4.3 (1.4-10)	3.8 (0.20-7.9)	3.6 (0.13-9.9)	5.0 (0.48-10)	.098
Preoperative MMSE	27 (21-28)	26 (20-29)	22 (11-28)	19 (10-27)	18 (4-27)	−.556**
APOE ε4	2 (50%)	15 (46%)	12 (60%)	12 (46%)	18 (49%)	.001
Initial shunt response	3 (75%)	29 (88%)	15 (75%)	17 (65%)	23 (62%)	−.217*
Shunt revision during follow up	1 (25%)	6 (18%)	1 (5.0%)	1 (3.8%)	2 (5.4%)	−.185*
Deceased during follow-up	1 (25%)	15 (46%)	11 (55%)	19 (32%)	12 (32%)	.053

Abbreviations: CDR-GS = Clinical Dementia Rating Global score (severity of cognitive impairment: 0 = healthy, 0.5 = very mild, 1 = mild, 2 = moderate, 3 = severe); MMSE = Mini-Mental State Examination (range 0-30, 30 indicating no deterioration in cognition). Variables are shown in median (range) or number (%).
[a] Spearman's correlation coefficient.
* Significant at $P < .05$ level.
** Significant at $P < .01$ level.

Immunohistochemistry

The frontal cortex biopsy samples were fixed in buffered formalin overnight and subsequently embedded in paraffin. Deparaffinized sections 5 μm thick were used for immunohistochemical staining. Antigen retrieval was performed by boiling the sections in 10 mM Tris-1 mM EDTA buffer, pH 9.0, in pressure cooker for 10 min, followed by cooling to room temperature and incubation in 80% formic acid for 20 min. Staining and imaging were performed by investigators blinded to sample identity. Control sections without the primary antibodies were processed simultaneously; no nonspecific staining was observed.

For staining of microglia (Iba1) and Aβ, endogenous peroxidase activity was quenched by incubation in 1% H_2O_2. Nonspecific antibody binding was blocked using 3% bovine serum albumin (BSA). Sections were incubated with rabbit polyclonal anti-Iba-1 (No. 019-19,741, 1:1500, FUJI-FILM Wako Chemicals Europe GmbH, Neuss, Germany) overnight at 4°C, followed by biotinylated anti-rabbit secondary antibody (1:200, Vector Laboratories, Burlingame, CA, United States) for 1 h and Vectastain Elite ABC Kit Peroxidase (Vector Laboratories). 3,3′-Diaminobenzidine (Sigma-Aldrich, St Louis, MO, United States) was used as chromogen for a 90-s incubation time. Staining of the second antigen was started with blocking with 3% BSA and incubation with mouse monoclonal anti-Aβ (anti-β-amyloid 17-24, clone 4G8, No. 800712, 1:500, Biolegend, San Diego, CA, United States) overnight at 4°C. Staining was visualized with biotinylated anti-mouse secondary antibody (1:200, Vector Laboratories) and Vectastain ABC-AP Kit (Vector Laboratories), and 30-min incubation with Permanent AP Red Kit substrate/chromogen (Zytomed Systems GmbH, Berlin, Germany). Sections were counterstained with Mayer's hematoxylin and mounted with aqueous mounting medium (Aquatex, Merck, Darmstadt, Germany) (Figure 2). Stained biopsy sections were imaged with Hamamatsu NanoZoomer XR Digital slide scanner, with magnification of x40, and with final resolution of 226 nm/pixel. Obtained WSIs were uploaded to Aiforia cloud platform.

For fluorescent triple staining of Iba-1, Aβ, and CD68, lipofuscin autofluorescence was quenched using TrueBlack lipofuscin autofluorescence quencher (No. 23007, Biotium Inc., Fremont, CA, United States), and nonspecific antibody binding was blocked using 5% BSA. The sections were incubated simultaneously with the following primary antibodies: rabbit monoclonal anti-CD68 (ab213363, Abcam, Cambridge, United Kingdom; 1:5000), mouse monoclonal anti-β-amyloid (clone 4G8, No. 800712, Biolegend; 1:500), and goat polyclonal anti-Iba-1 (ab5076, Abcam; 1:1000), followed by incubation with the following secondary antibodies: biotinylated horse anti-rabbit (1:200, BA-1100-1.5, Vector Laboratories), Alexa Fluor 568 Donkey anti-Mouse IgG (H + L) (1:500, A-10037, Thermo Scientific, Waltham, MA, United States), and Alexa Fluor 633 Donkey anti-Goat IgG (H + L) (1:500, A-21082 Thermo Scientific). Following antibody incubations, CD68 was visualized by tyramide signal amplification, using Alexa Fluor 488 Tyramide SuperBoost Kit, streptavidin (B40932, Invitrogen, Waltham, MA, United States) with 5 min incubation of the tyramide solution. Sections were counterstained with DAPI (1 μg/mL) and mounted with Vectashield Antifade Mounting Medium (H-1000-10, Vector Laboratories). Whole slide fluorescent images were obtained with Olympus VS200 slide scanning microscope equipped with VS-304M camera. 20x magnifying objective was used with final resolution of 345 nm/pixel.

CNN model (Iba1/4G8)

Training annotations in Aiforia cloud platform for 4 CNN models were made (by A.J.L.) on 27 WSIs to detect brain tissue, Aβ area within brain tissue, non-Aβ area within brain tissue, and microglia somas both within Aβ and non-Aβ area (Figure 3). WSIs for the training dataset were chosen to represent all variations, eg, staining intensity, within the cohort samples. Final training of all CNNs included all training data and a maximum of 1500 iterations. Performance of the Iba1/4G8 model was evaluated after each training, and training annotations were refined to achieve the final model. Aiforia
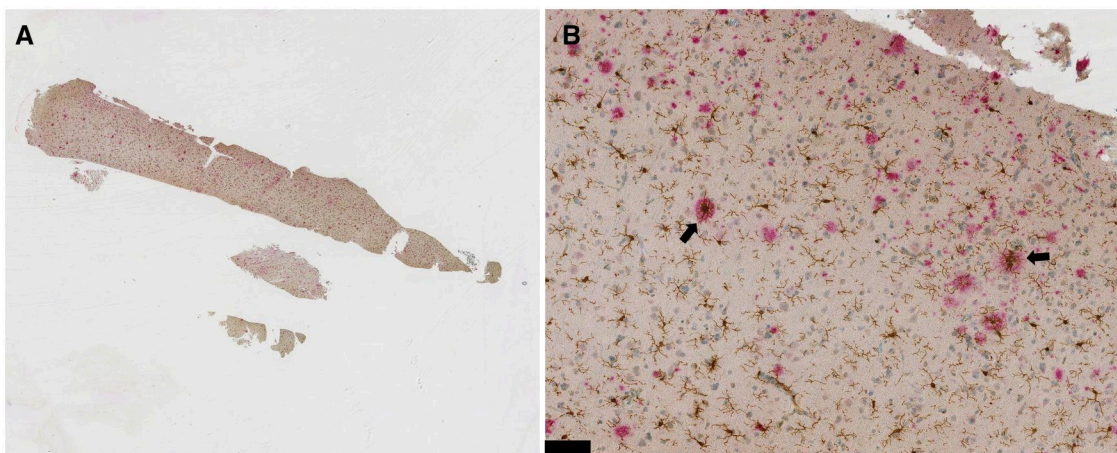

Figure 2. (A) Iba1 (microglia, brown)/4G8 (β-amyloid, pink) double-staining of frontal cortical biopsy. (B) Plaque-associated microglia (arrows). Scale bar: 100 μm.
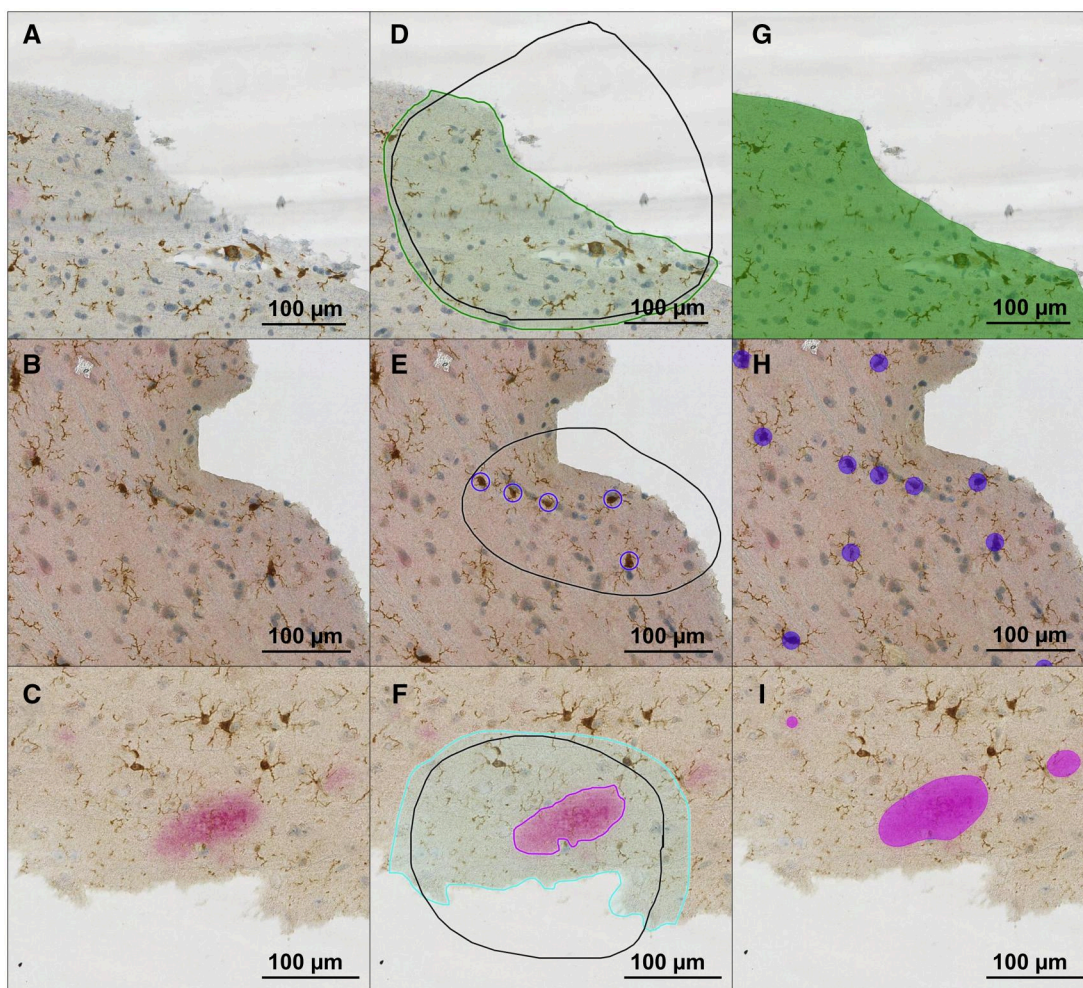
Figure 3. Training of the convoluted neural network (CNN) model for Iba1/4G8 stained frontal cortical biopsies. (A-C) baseline Iba1 (microglia, brown)/4G8 (Aβ, pink) stain. (D) Training annotation for tissue. (E) Training annotation for microglia somas. (F) Training annotation for Aβ area. (G) Final CNN model for automated tissue detection. (H) Final CNN model for automated microglia soma detection. (I) Final CNN model for automated Aβ-area detection.

cloud platform provided performance statistics for each model. The final CNN model was used to analyze the 120 WSIs of the study population. As a baseline, whole tissue area of the sample in the WSI was included in the region of interest (ROI) for the analysis. Tissue with severe fixation problems or major artifacts were excluded from the ROIs. Tissue for ROIs was available for all samples. After image analysis, amount of microglia somas within 25 μm from Aβ area (center of the microglia soma to border of Aβ area) was obtained via spatial distribution metrics.

CNN model (Iba1/4G8/CD68)

Training annotations in Aiforia cloud platform for 4 CNN models were made (by A.J.L.) on 26 WSIs to detect brain tissue, Aβ area within brain tissue, non-Aβ area within brain tissue, and microglia somas with CD68 positivity both within Aβ and non-Aβ area (Figure 4). WSIs for the training dataset were chosen to represent all variation, eg, staining intensity, within the cohort samples.

Statistics

IBM SPSS Statistic 27.0 for Windows software was used for statistical analyses. Cohort data is presented as number with percentage for categorical variables and median with range for continuous variables. Comparisons between groups were done with the Fisher exact test for categorical variables and with Mann-Whitney *U*-test for continuous variables. Spearman's correlation was calculated to find statistical dependence between CDR-GS and variables.

To adjust for confounding factors, binomial logistic regression was applied for the development of major neurodegenerative disorder and ACS and ordinal logistic regression with likelihood ratio test was applied for CDR-GS. Variables for regression model were chosen as follows: age at the time of shunt surgery, sex, presence of *APOE* ε4 allele, and Aβ area coverage. Preoperative MMSE was left out of the model due to its prominent correlation with the clinical diagnosis of dementia, ACS, and CDR-GS. Hosmer-Lemeshow test was used to determine goodness-of-fit of the binary regression
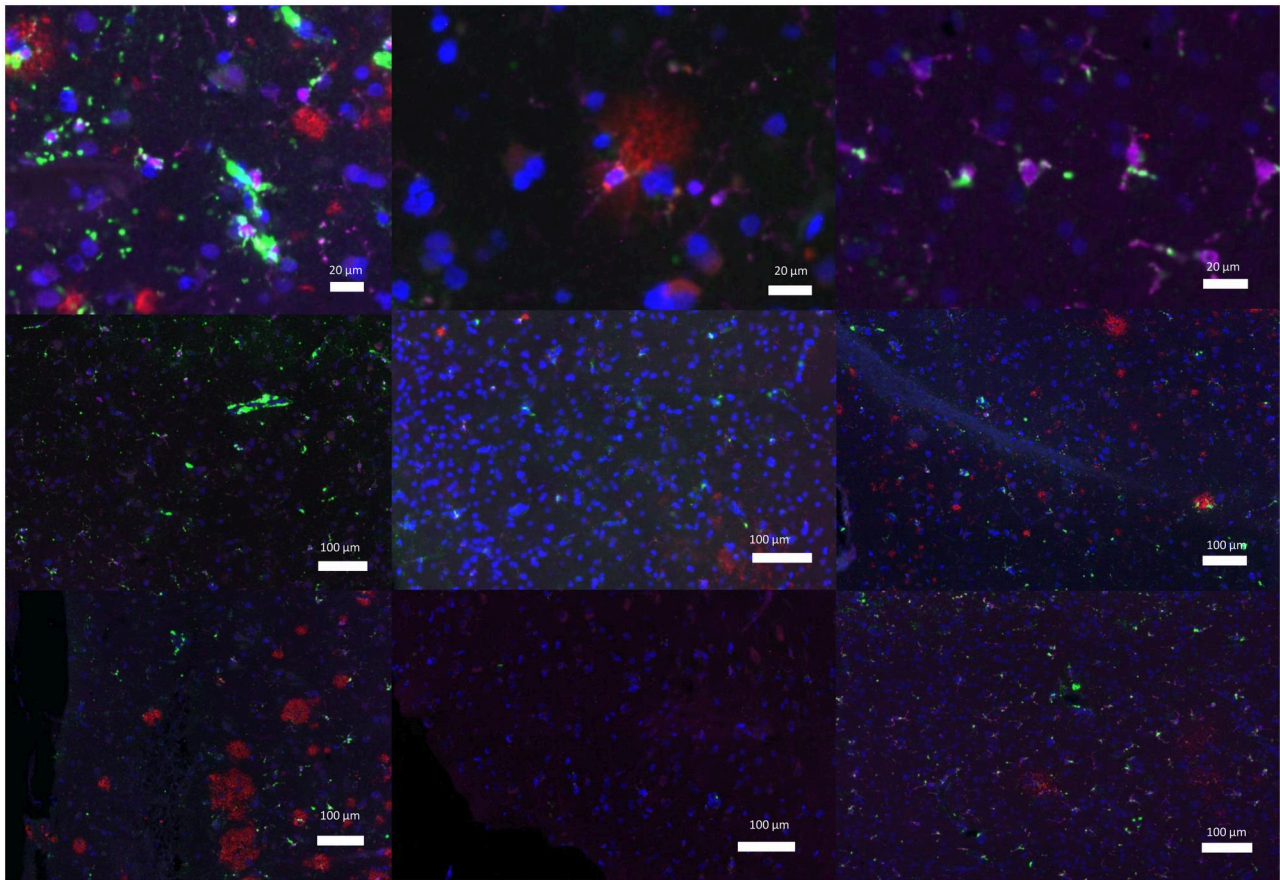
Figure 4. Iba1 (microglia, pink)/4G8 (Aβ, red)/CD68 (lysosomes, green) triple staining of 9 different frontal cortical biopsies, showing significant heterogeneity among the samples.

models, and Pearson's chi-square for goodness-of-fit of the ordinal regression model. *P*-values of $<.05$ were considered significant across all statistical analyses.

RESULTS

Performance of the CNN models

We developed CNN models to quantify Aβ area and Aβ-associated microglia in frontal cortex brain biopsy tissue samples obtained during shunt surgery to treat iNPH. We first trained CNNs for sections double labeled for Aβ and pan-microglial marker Iba-1 using traditional chromogen stains (Figure 3). Precision for tissue, Aβ-area, and microglia somas was excellent ($>95\%$) in training set (27 WSI) and total error for area or object was regarded as acceptable. However, the model tended to overestimate Aβ area (highest false-positive rate approximately ~25%) (Table 4). We next aimed to assess the feasibility of CNNs to analyze multiplexed immunofluorescence staining, which allows simultaneous detection of 3 or more targets in the same tissue section and thus provides invaluable information on the spatial organization and co-expression of the targets. To refine the analysis of Aβ-associated microglia, we included CD68, which labels the lysosomes of macrophage-lineage cells and is a commonly used marker of microglial activation. Following the gold standard of imaging immunofluorescence staining, laser intensities and acquisition times were kept constant for all the sections. However, due to heterogeneity of the staining intensity (Figure 4), the CNN model was unable to recognize CD68-positive microglia with reliable accuracy in a set of up to 242 individual training areas, yielding only precision of 77% and F1 score of 86%. Because precision was not improved by further training, ie, by refining, adjusting, or adding training areas, the model was deemed futile and analyses for the whole study population were not conducted. However, precision of tissue and Aβ-area recognition were comparable to Iba1/4G8 model (Table 4). Together, our results suggest that CNN models perform well on chromogen immunohistochemical stains but may not be easily adapted for multiplexed immunofluorescence staining.

Cohort characteristics

Our study cohort included 120 individuals with Aβ positive frontal cortex biopsy obtained during a shunt surgery to treat iNPH. Clinical endpoints to assess progression of dementing diseases were: (1) diagnosed ACS to evaluate day-to-day clinicians' point-of-view; (2) development of dementia (major neurodegenerative disorder) as dichotomized entity regardless of etiology for the dementing disease; and (3) the CDR-GS to address the severity of dementing disease on ordinal scale. At the end of the follow-up (median period of 4.4 years), 84

Table 4. Performance of the CNN models.

	Total area/object error	Precision	Sensitivity	Highest class-specific error (FP%/FN%)
Iba1/4G8				
Tissue	0.58%	99.6%	99.3%	1.10% (0.43%/0.67%)
Aβ area	4.34%	97.9%	96.8%	
Aβ area				32.4% (25.2%/7.20%)
Non-Aβ area				3.44% (0.53%/2.91%)
Microglia soma	6.12%	96.5%	97.5%	6.12% (3.59%/2.53%)
Iba1/4G8/CD68				
Tissue	0.89%	98.9%	99.5%	1.61% (1.13%/0.48%)
Aβ area	1.59%	99.5%	98.8%	
Aβ area				24.4% (22.5%/1.89%)
Non-Aβ area				1.21% (0.07%/1.14%)
Microglia soma	31.8%	76.9%	97.6%	31.8% (29.4%/2.38%)

Performance of convoluted neural network model to detect frontal cortical biopsy samples for brain tissue, Aβ area, non-Aβ area, and microglia somas. Total Aβ area was acquired by combining automated detection of Aβ area and non-Aβ area.

Table 5. Variables acquired with automated WSI analysis using the microglia/Aβ-model.

	Microglia soma density (count/mm^2)	P-value	Aβ-related microglia density (count/mm^2)	P-value	Aβ area coverage (%)	P-value
Dementia n = 84	75.1 (39.5-165)	.950[a]	362 (93.7-863)	.873[a]	4.73 (0.13-53.2)	.002[a]
No dementia n = 36	75.9 (23.3-161)		407 (0-1760)		1.56 (0-39.1)	
ACS n = 46	70.6 (40.0-132)	.246[a]	348 (93.7-716)	.524[a]	6.55 (0.18-53.2)	<.001[a]
No ACS n = 74	78.0 (23.3-165)		393 (0-1760)		2.29 (0-39.1)	
CDR-GS						
0	86.9 (75.5-165)	.569[b]	383 (174-772)	.386[b]	1.61 (0.13-39.1)	.007[b]
0.5	76.4 (23.3-161)	($r_s = -.052$)	406 (0-1760)	($r_s = .080$)	1.52 (0-23.5)	($r_s = .246$)
1	74.7 (46.6-114)		331 (129-658)		4.32 (0.58-28.6)	
2	71.6 (39.5-139)		355 (93.7-790)		5.54 (0.55-53.2)	
3	76.0 (45.2-132)		387 (94.3-863)		4.43 (0.18-20.0)	

Abbreviations: WSI = whole slide image; ACS = Alzheimer's clinical syndrome; CDR-GS = Clinical Dementia Rating Global score (severity of cognitive impairment: 0 = healthy, 0.5 = very mild, 1 = mild, 2 = moderate, 3 = severe).
Variables are shown in median (range).
[a] Mann–Whitney *U*-test.
[b] Spearman's correlation *P* (r_s).

(70%) patients were diagnosed with a major neurodegenerative disorder (Table 1). ACS was observed in 46 patients (38%) (Table 2). Patients who developed major neurodegenerative disorder were older (P = .003) and had lower baseline MMSE (P<.001) and had worse results from ventriculoperitoneal shunting (P = .008). CDR-GS at the end of follow-up had a weak positive correlation to the age at the time of shunt ($r_s = .245$), a moderate negative correlation to the preoperative MMSE ($r_s = -.556$), a weak negative correlation to observed shunt response ($r_s = -.217$), and a weak negative correlation to shunt revision during follow-up ($r_s = -.185$) (Table 3). Older age at the time of shunt surgery was also a discriminating factor among patients with observed ACS at the end of follow-up (P = .001); and they also had lower baseline MMSE (P<.001) (Table 2). Patients without observed ACS had higher rate of shunt revisions (P = .049) (Table 2).

Association between cognitive outcome and CNN-derived Aβ and microglia measures

Microglia soma density (count per mm^2), Aβ-associated microglia density (count per Aβ area mm^2), and Aβ area coverage (percentage of tissue detected) were acquired from the WSIs of the whole study cohort and analyzed in relation to cognitive outcome at the end of follow-up. There were no significant differences between groups either in mean microglia soma density or Aβ-related microglia density and no significant correlations were observed (Table 5).

Patients with major neurodegenerative disorder (P = .002) and ACS had higher coverage of Aβ in biopsy samples (P<.001), and a similar trend was observed with CDR-GS having a weak correlation to Aβ coverage ($r_s = .246$) (Table 5). Aβ area coverage was categorized according to quartiles (Q1 = 1.49%, Q2 = 3.59%, Q3 = 9.31%), which were further rationalized into 4 groups (<1%, 1%-4.9%, 5%-10%, and >10%) for the analysis to increase readability and ease interpretation. Association of Aβ coverage by rationalized quartiles is shown for major neurodegenerative disorder (Figure 5A; Table 6), ACS (Figure 5B; Table 7), and proportionally for CDR-GS (Figure 5C; Table 8). When adjusted for sex and the presence of *APOE* ε4 allele, we found that age at the time of shunting and Aβ coverage were potential independent risk factors: (1) higher Aβ coverage predicted development of major neurodegenerative disorder (dementia), diagnosis of ACS, and more severe memory disease when
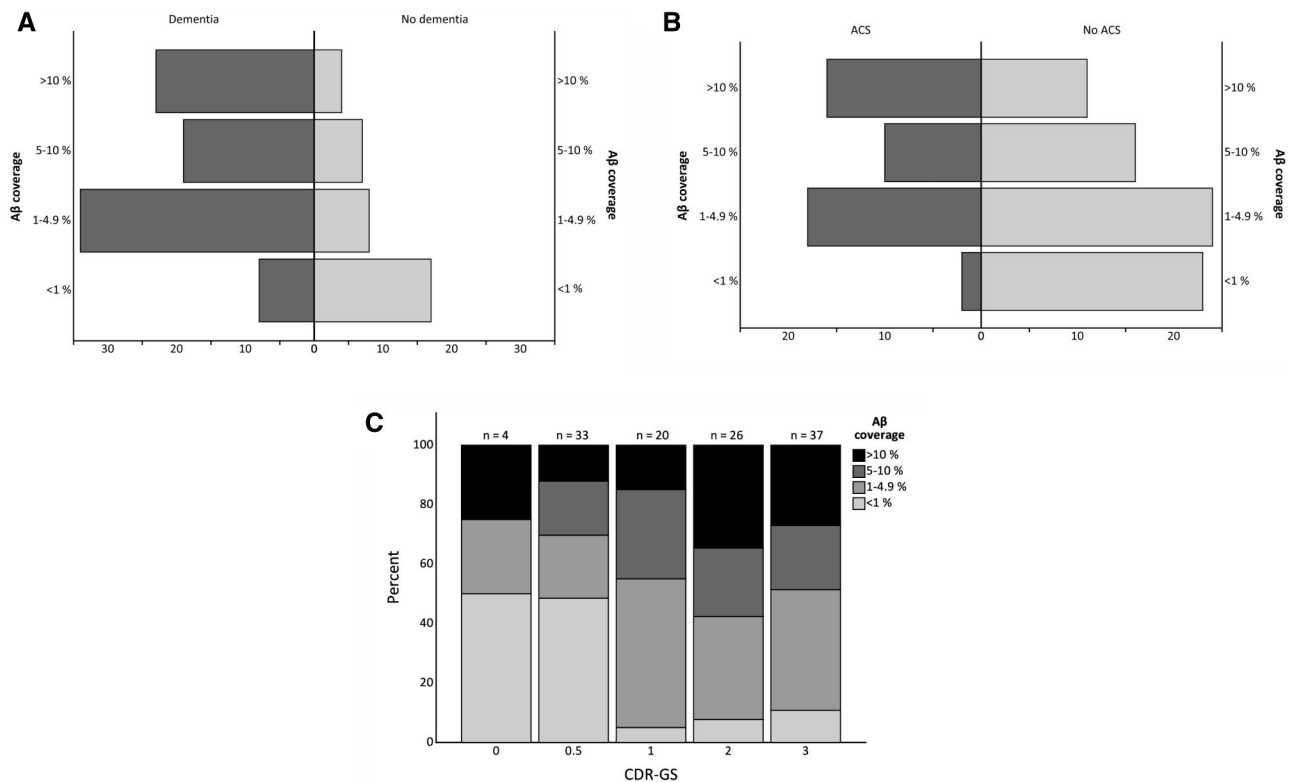
Figure 5. (A) Distribution of Aβ coverage by major neurodegenerative disorder (dementia). Number of patients is shown on *X*-axis. Binary logistic regression model for development of dementia was done with Aβ area coverage, age at shunt operation, sex, and *APOE* ε4, yielding OR 1.7 (1.1-2.7) for Aβ area coverage and OR 1.1 (1.0-1.2) for age at shunt operation. (B) Distribution of Aβ coverage by Alzheimer disease clinical syndrome (ACS). Number of patients is shown on *X*-axis. Binary logistic regression model for development of ACS was done with Aβ area coverage, age at shunt operation, sex, and *APOE* ε4, yielding OR 1.7 (1.1-2.5) for Aβ area coverage and OR 1.1 (1.0-1.2) for age at shunt operation. (C) Proportional Aβ coverage by Clinical Dementia Rating Global score. CDR-GS, Clinical Dementia Rating Global score (severity of cognitive impairment: 0 = healthy, 0.5 = very mild, 1 = mild, 2 = moderate, 3 = severe). Ordinal logistic regression model for CDR Global Score was done with Aβ area coverage, age at shunt operation, sex, and *APOE* ε4, yielding OR 1.5 (1.1-2.1) for Aβ area coverage and OR 1.1 (1.0-1.2) for age at shunt operation.

Table 6. Regression model for development of major neurodegenerative disorder (dementia).

	Dementia $n = 84$	No dementia $n = 36$	P-value[a]	OR[b]	CI[b]
Aβ coverage			.016	1.739	1.107-2.732
<1%	8 (9.5%)	17 (47%)			
1-4.9%	34 (41%)	8 (22%)			
5-10%	19 (23%)	7 (19%)			
>10%	23 (27%)	4 (11%)			
Age at shunt operation (years)	79.0 (64.4-88.3)	76.2 (62.5-87.3)	.011	1.126	1.028-1.234

Variables are shown in median (range), or number (%).
[a] Chi-square test was used for categorical variables, Mann–Whitney *U*-test for continuous.
[b] Binary logistic regression model including Aβ area coverage, age at shunt operation, sex, and *APOE* ε4.

measured with CDR-GS; and (2) higher age at the time of shunting was associated with development of major neurodegenerative disorder (dementia), diagnosis of ACS, and more severe memory disease when measured with CDR-GS. Hosmer–Lemeshow test for goodness-of-fit was insignificant across binary regression models, and Pearson's chi-square for goodness-of-fit was insignificant for ordinal regression model, both indicating good fit of the used data to the model.

DISCUSSION

In this retrospective cohort study, we built a CNN-based AI model for automated detection of Aβ and microglia somas in frontal cortical biopsies. We then correlated the development of major neurodegenerative disorder and the severity of memory disease by CDR-GS to the quantified amount of Aβ, microglia density, and Aβ-related microglia reaction. To the best of our knowledge, this is the first attempt to predict

Table 7. Regression model for Alzheimer disease clinical syndrome (ACS) on follow-up.

	ACS $n = 46$	No ACS $n = 74$	P-value[a]	OR[b]	CI[b]
Aβ coverage			.012	1.681	1.122-2.521
<1%	2 (4.3%)	23 (31%)			
1-4.9%	18 (39%)	24 (32%)			
5-10%	10 (22%)	16 (22%)			
>10%	16 (35%)	11 (15%)			
Age at shunt operation (years)	80.3 (64.5-88.3)	77.6 (62.5-87.6)	.017	1.120	1.020-1.228

Variables are shown in median (range) or number (%).
[a] Chi-square test was used for categorical variables, Mann–Whitney *U*-test for continuous.
[b] Binary logistic regression model including Aβ area coverage, age at shunt operation, sex, and *APOE* ε4.

Table 8. Regression model for Clinical Dementia Rating Global score at the end of follow-up.

CDR-GS	0 $n = 4$	0.5 $n = 33$	1 $n = 20$	2 $n = 26$	3 $n = 37$	r_s[a]	OR[b]	CI[b]
Aβ coverage						.276*	1.502	1.068-2.114
<1%	2 (50%)	16 (49%)	1 (5%)	2 (8%)	4 (11%)			
1-4.9%	1 (25%)	7 (21%)	10 (50%)	9 (35%)	15 (41%)			
5-10%	0 (0%)	6 (18%)	6 (30%)	6 (23%)	8 (22%)			
>10%	1 (25%)	4 (12%)	3 (15%)	9 (35%)	10 (23%)			
Age at shunt operation (years)	73.0 (69.0-79.5)	76.5 (62.5-87.3)	78.4 (64.4-87.2)	79.1 (68.8-88.3)	79.7 (64.5-87.6)	.245*	1.079	1.004-1.159

Abbreviation: CDR-GS = Clinical Dementia Rating Global score (severity of cognitive impairment: 0 = healthy, 0.5 = very mild, 1 = mild, 2 = moderate, 3 = severe).
Variables are shown in median (range), or number (%).
[a] Spearman's correlation coefficient.
[b] Ordinal logistic regression model including Aβ area coverage, age at shunt operation, sex, and *APOE* ε4.
* Significant at $P < .01$ level.

cognitive outcome in an in vivo cohort using automated, quantitative detection of Aβ, microglia, and Aβ-related microglia in shunted iNPH patients.

Most CNN models reported so far are used to analyze a single target in light-microscopy images. The ability to visualize multiple targets simultaneously in the same tissue section is vital when studying co-expression and spatial organization within the tissue architecture or when the sample material is limited. Our results indicate that CNN models can easily be adapted to analysis of WSI double labeled with chromogenic or fluorescent stains. We obtained similar results for Aβ load and Aβ-associated microglia analysis from both chromogenic and fluorescent staining, thereby validating our results. However, analysis of a marker of activated microglia intracellular CD68 stained in the same sections with Aβ and pan-microglial marker Iba-1 was beyond the capacity of the CNN model used. Analysis of chromogenic single stain of CD68 could be used to obtain crude CD68 load per section,[26] but would lack detailed information such as vicinity to Aβ plaques and identity of CD68-positive cells, since in addition to microglia, infiltrating macrophages and monocytes may contribute to detected CD68 load in the brain.

Our main finding is that quantitative assessment of Aβ load can be indicative of the severity of memory disorder, development of ACS, and dementia on follow-up of shunted iNPH patients. Build-up of Aβ is a well-known phenomenon in the natural course of AD, but previous studies done with tau and Aβ PET-imaging have shown that the accumulation of tau is more closely related to subsequent cognitive function than Aβ itself.[37] Furthermore, longitudinal tau-PET scans have been proposed to track the progression of the disease.[38] This is also reflected in our study, as the Aβ coverage was more correlated to dichotomized categorization of cognition, ie, the presence or absence of dementia or ACS, than the more detailed CDR Global Score. Although the brain biopsy sample represents only a small cortical area, the histological assessment of a sample can be more versatile than Aβ PET, as it illustrates a wider spectrum of Aβ accumulation from stellate lesions to diffuse and compact plaques and cerebral amyloid angiopathy. CSF total tau and neurofilament light protein associated with postoperative MMSE in iNPH patients in a study partly consisting of the same patient cohort.[39] However, the brain biopsy used in the current study represents a direct rather than an indirect indication of AD pathology, thereby providing improved accuracy. In addition, our current study provides long follow-up, more robust cognitive assessment, and the clinical diagnosis of AD. The fact that cognitive outcome can be addressed with a small local cortical biopsy underlines the global, diffuse nature of AD.

Genetic studies have indicated microglia as key contributors to AD pathogenesis[6,40,41] and reduced microglial clustering around Aβ plaques has been shown in AD patients carrying AD-associated *TREM2* variants[10,14,42] and in diabetic iNPH patients.[13] In the current study, neither overall nor Aβ associated microglia soma density seemed to act as an independent risk factor for the clinical outcome when measured as a bulk.

Our findings are in accordance with a previous study in an NPH cohort that concluded that microglial gene expression was correlated with plaque association and microglial morphology but not cognitive status.[43] Microglia are highly dynamic cells and can adopt a variety of different activation states in response to stimuli in their microenvironment. Transcriptional signatures of different microglial states such as disease-associated microglia have been extensively studied in mouse models of AD but often have limited overlap with transcriptional signatures detected in microglia from postmortem brains of AD patients.[44,45] Currently, there are no well-established markers that would specifically label distinct microglial cell populations. Iba1 has long been considered as a pan-microglial marker that can be used to identify microglial cells irrespective of their phenotype or activation state.[46,47] Although a more recent study suggests that Iba1 is not expressed by all microglial cells, the study found that the majority of the microglia surrounding or infiltrating Aβ plaques were immunopositive for Iba1.[48] Since our aim was to quantitate the plaque-associated microglia, we used an antibody against Iba1 to label the microglial cells. CD163 has been suggested as a marker for amyloid-responsive microglia.[9] However, since CD163 is highly expressed by parenchymal border macrophages[49] and brain-invaded monocyte-derived cells,[50] co-labeling with other microglial markers may be necessary to differentiate CD163-expressing microglia from these other cell populations. Thus, stratification according to genes that modify microglial reactions, Aβ plaque, and microglia morphology as well as specific markers identifying Aβ-reactive microglia,[9] in addition to vicinity to Aβ plaque should be considered in future automated analyses.

The diffuse nature of Aβ plaques and subtle Aβ staining is a true challenge when analyzing WSIs. The threshold to determine Aβ area for training annotations is extremely challenging for the human eye, and accounts for relatively high Aβ-area false positive rate in our automated analysis. However, this is a known feature of the model developed as automated analysis is used specifically for challenging tasks, not those obvious to the human eye. Consequently, this was observed in WSI analysis systematically and was not considered as an obstacle to further analysis and correlation with the clinical outcome. Overall precision of the Aβ/microglia model was considered adequate, as the total area and object recognition errors were in line with the previous CNN models developed and the inter-observer error among pathologists.[51,52]

Accuracy of the clinical diagnosis of AD impacts heavily on the conclusions that can be made from our findings of ACS.[53] Findings in our cohort are feasible, as fewer cases of ACS were diagnosed during the follow-up than there were demented patients at the end of follow-up and dementia also from other causes than AD is expected in iNPH population.[21] It is noteworthy that patients with eventual ACS undergo fewer shunt revisions, although they have close to equal frequency of initial shunt response. This underlines that these patients most likely have other comorbid neurodegenerative processes in addition to chronic hydrocephalus.[21,54,55] Very few Aβ-positive iNPH patients remain cognitively intact in a median of 4.4 years of follow-up, even despite evidently normal cognition at the time

of the shunt. However, cognitive decline at the time of the shunt (as expected), seems to predict further cognitive deterioration.[21,56] We selected only Aβ-positive patients since the main aim was to predict development of ACS. We are also aware that patients with negative Aβ pathology can develop major neurodegenerative disorders with high frequency but this is even more often related to causes other than AD. Also, the cortical biopsy represents only a small area of tissue and early Aβ pathology can be patchy, and therefore inadvertently ignored.

The insignificance of *APOE* genotype among development of major neurodegenerative disorder, ACS, and cognitive outcome is likely due to the fact that the study population consists solely of patients with positive Aβ biopsies at baseline evaluation (Tables 1-3). CSF AD biomarkers correlate with Aβ load in cortical biopsies in iNPH patients,[57,58] but these should be interpreted with caution in the iNPH population.[59–61] Thus, the reliability of CSF biomarkers is challenged, emphasizing the relevance of diagnostic brain biopsy during shunt surgery in iNPH.[62]

The strengths of our study include a large real-life patient cohort, long follow-up time, and state-of-the-art AI using a CNN model. The fact that microglia and Aβ-related microglia were analyzed as bulk hampers our ability to draw conclusions regarding the relation of microglia to the development of AD. Further studies that consider microglia morphology and activity by genetic analysis are endorsed.

In conclusion, we determined that quantitative analysis of Aβ coverage and amounts of microglia with AI using a CNN model was feasible. Higher Aβ coverage in cortical biopsies seemed to correlate with CDR-GS and the development of ACS and dementia. However, microglial density and Aβ-related microglia did not correlate with cognitive outcome when measured as a bulk.

DATA AVAILABILITY

The datasets used and/or analyzed during the current study will be available from the corresponding author on reasonable request.

CONFLICTS OF INTEREST

None declared.

REFERENCES

1. Scheltens P, De Strooper B, Kivipelto M, et al. Alzheimer's disease. *Lancet*. 2021;397:1577-1590.
2. Jack CR, Bennett DA, Blennow K, et al. NIA-AA Research Framework: toward a biological definition of Alzheimer's disease. *Alzheimers Dement*. 2018;14:535-562.
3. Jack CR, Knopman DS, Jagust WJ, et al. Hypothetical model of dynamic biomarkers of the Alzheimer's pathological cascade. *Lancet Neurol*. 2010;9:119-128.
4. Cohen AD, Landau SM, Snitz BE, et al. Fluid and PET biomarkers for amyloid pathology in Alzheimer's disease. *Mol Cell Neurosci*. 2019;97:3-17.
5. Bellenguez C, Charbonnier C, Grenier-Boley B, et al.; CNR MAJ Collaborators. Contribution to Alzheimer's disease risk of rare variants in TREM2, SORL1, and ABCA7 in 1779 cases and 1273 controls. *Neurobiol Aging*. 2017;59:220.e1-220-e9.
6. Sims R, van der Lee SJ, Naj AC, et al. Rare coding variants in PLCG2, ABI3, and TREM2 implicate microglial-mediated innate immunity in Alzheimer's disease. *Nat Genet*. 2017;49:1373-1384.
7. Keren-Shaul H, Spinrad A, Weiner A, et al. A unique microglia type associated with restricting development of Alzheimer's disease. *Cell*. 2017;169:1276-1290.e17.
8. Sala Frigerio C, Wolfs L, Fattorelli N, et al. The major risk factors for Alzheimer's disease: age, sex, and genes modulate the microglia response to Aβ plaques. *Cell Rep*. 2019;27:1293-1306.e6.
9. Nguyen AT, Wang K, Hu G, et al. APOE and TREM2 regulate amyloid-responsive microglia in Alzheimer's disease. *Acta Neuropathol*. 2020;140:477-493.
10. Yuan P, Condello C, Keene CD, et al. TREM2 haplodeficiency in mice and humans impairs the microglia barrier function leading to decreased amyloid compaction and severe axonal dystrophy. *Neuron*. 2016;90:724-739.
11. Wang Y, Ulland TK, Ulrich JD, et al. TREM2-mediated early microglial response limits diffusion and toxicity of amyloid plaques. *J Exp Med*. 2016;213:667-675.
12. Parhizkar S, Arzberger T, Brendel M, et al. Loss of TREM2 function increases amyloid seeding but reduces plaque-associated ApoE. *Nat Neurosci*. 2019;22:191-204.
13. Natunen T, Martiskainen H, Marttinen M, et al. Diabetic phenotype in mouse and humans reduces the number of microglia around β-amyloid plaques. *Mol Neurodegener*. 2020;15:66.
14. Prokop S, Miller KR, Labra SR, et al. Impact of TREM2 risk variants on brain region-specific immune activation and plaque microenvironment in Alzheimer's disease patient brain samples. *Acta Neuropathol*. 2019;138:613-630.
15. Zaccaria V, Bacigalupo I, Gervasi G, et al. A systematic review on the epidemiology of normal pressure hydrocephalus. *Acta Neurol Scand*. 2020;141:101-114.
16. Relkin N, Marmarou A, Klinge P, et al. Diagnosing idiopathic normal-pressure hydrocephalus. *Neurosurgery*. 2005;57:S4-S16.
17. Leinonen V, Koivisto AM, Savolainen S, et al. Post-mortem findings in 10 patients with presumed normal-pressure hydrocephalus and review of the literature. *Neuropathol Appl Neurobiol*. 2012;38:72-86.
18. Fasano A, Espay AJ, Tang-Wai DF, et al. Gaps, controversies, and proposed roadmap for research in normal pressure hydrocephalus. *Mov Disord*. 2020;35:1945-1954.
19. Wikkelsø C, Hellström P, Klinge PM, et al.; European iNPH Multicentre Study Group. The European iNPH Multicentre Study on the predictive values of resistance to CSF outflow and the CSF tap test in patients with idiopathic normal pressure hydrocephalus. *J Neurol Neurosurg Psychiatry*. 2013;84:562-568.
20. Nakajima M, Yamada S, Miyajima M, et al.; SINPHONI-2 Investigators. Tap test can predict cognitive improvement in patients with iNPH-results from the multicenter prospective studies SINPHONI-1 and -2. *Front Neurol*. 2021;12:769216.
21. Koivisto AM, Alafuzoff I, Savolainen S, et al.; Kuopio NPH Registry (www.uef.finph). Poor cognitive outcome in shunt-responsive idiopathic normal pressure hydrocephalus. *Neurosurgery*. 2013;72:1-8;discussion 8.
22. Nerg O, Junkkari A, Hallikainen I, et al. The CERAD neuropsychological battery in patients with idiopathic normal pressure hydrocephalus compared with normal population and patients with mild Alzheimer's disease. *J Alzheimers Dis*. 2021;81:1117-1130.
23. Luikku AJ, Hall A, Nerg O, et al. Predicting development of Alzheimer's disease in patients with shunted idiopathic normal pressure hydrocephalus. *J Alzheimers Dis*. 2019;71:1233-1243.
24. Gazestani V, Kamath T, Nadaf NM, et al. Early Alzheimer's disease pathology in human cortex involves transient cell states. *Cell*. 2023;186:4438-4453.e23.
25. Perosa V, Scherlek AA, Kozberg MG, et al. Deep learning assisted quantitative assessment of histopathological markers of Alzheimer's disease and cerebral amyloid angiopathy. *Acta Neuropathol Commun*. 2021;9:141.
26. Auger CA, Perosa V, Greenberg SM, et al. Cortical superficial siderosis is associated with reactive astrogliosis in cerebral amyloid angiopathy. *J Neuroinflammation*. 2023;20:195.
27. Penttinen AM, Parkkinen I, Blom S, et al. Implementation of deep neural networks to count dopamine neurons in substantia nigra. *Eur J Neurosci*. 2018;48:2354-2361.
28. Sjöblom N, Boyd S, Manninen A, et al. Chronic cholestasis detection by a novel tool: automated analysis of cytokeratin 7-stained liver specimens. *Diagn Pathol*. 2021;16:41.
29. Aiforia Technologies Oyj. Aiforia [Internet]. 2024. Accessed June 25, 2024. https://www.aiforia.com/
30. Junkkari A, Luikku AJ, Danner N, et al. The Kuopio idiopathic normal pressure hydrocephalus protocol: initial outcome of 175 patients. *Fluids Barriers CNS*. 2019;16:21.
31. Hänninen JJ, Nakajima M, Vanninen A, et al. Neuropathological findings in possible normal pressure hydro-cephalus: a postmortem study of 29 cases with lifelines. *Free Neuropathol*. 2022;3:3-2.
32. Malm J, Jacobsson J, Birgander R, et al. Reference values for CSF outflow resistance and intracranial pressure in healthy elderly. *Neurology*. 2011;76:903-909.
33. Dubois B, Feldman HH, Jacova C, et al. Research criteria for the diagnosis of Alzheimer's disease: revising the NINCDS-ADRDA criteria. *Lancet Neurol*. 2007;6:734-746.
34. Morris JC. The Clinical Dementia Rating (CDR): current version and scoring rules. *Neurology*. 1993;43:2412-2414.
35. Sachdev PS, Blacker D, Blazer DG, et al. Classifying neurocognitive disorders: the DSM-5 approach. *Nat Rev Neurol*. 2014;10:634-642.
36. Pyykko OT, Helisalmi S, Koivisto AM, et al. APOE4 predicts amyloid- in cortical brain biopsy but not idiopathic normal pressure hydrocephalus. *J Neurol Neurosurg Psychiatry*. 2012;83:1119-1124.
37. Brier MR, Gordon B, Friedrichsen K, et al. Tau and Aβ imaging, CSF measures, and cognition in Alzheimer's disease. *Sci Transl Med*. 2016;8:338ra66.
38. Harrison TM, La Joie R, Maass A, et al. Longitudinal tau accumulation and atrophy in aging and Alzheimer disease. *Ann Neurol*. 2019;85:229-240.
39. Lukkarinen H, Jeppsson A, Wikkelsö C, et al. Cerebrospinal fluid biomarkers that reflect clinical symptoms in idiopathic normal pressure hydrocephalus patients. *Fluids Barriers Cns*. 2022;19:11.
40. Schwartzentruber J, Cooper S, Liu JZ, et al. Genome-wide meta-analysis, fine-mapping and integrative prioritization implicate new Alzheimer's disease risk genes. *Nat Genet*. 2021;53:392-402.
41. Bellenguez C, Küçükali F, Jansen IE, et al.; CHARGE. New insights into the genetic etiology of Alzheimer's disease and related dementias. *Nat Genet*. 2022;54:412-436.

42. Parhizkar S, Arzberger T, Brendel M, et al. Loss of TREM2 function increases amyloid seeding but reduces plaque-associated ApoE. *Nat Neurosci*. 2019;22:191-204.

43. Huang W, Bartosch AM, Xiao H, et al. An immune response characterizes early Alzheimer's disease pathology and subjective cognitive impairment in hydrocephalus biopsies. *Nat Commun*. 2021;12:5659.

44. Chen Y, Colonna M. Microglia in Alzheimer's disease at single-cell level. Are there common patterns in humans and mice? *J Exp Med*. 2021;218:e20202717.

45. Sun N, Victor MB, Park YP, et al. Human microglial state dynamics in Alzheimer's disease progression. *Cell*. 2023;186:4386-4403.e29.

46. Ito D, Imai Y, Ohsawa K, et al. Microglia-specific localisation of a novel calcium binding protein, Iba1. *Brain Res Mol Brain Res*. 1998;57:1-9.

47. Walker DG, Lue LF. Immune phenotypes of microglia in human neurodegenerative disease: challenges to detecting microglial polarization in human brains. *Alzheimers Res Ther*. 2015;7:56.

48. Kenkhuis B, Somarakis A, Kleindouwel LRT, et al. Co-expression patterns of microglia markers Iba1, TMEM119 and P2RY12 in Alzheimer's disease. *Neurobiol Dis*. 2022;167:105684.

49. Drieu A, Du S, Storck SE, et al.; Dominantly Inherited Alzheimer Network. Parenchymal border macrophages regulate the flow dynamics of the cerebrospinal fluid. *Nature*. 2022;611:585-593.

50. Muñoz-Castro C, Mejias-Ortega M, Sanchez-Mejias E, et al. Monocyte-derived cells invade brain parenchyma and amyloid plaques in human Alzheimer's disease hippocampus. *Acta Neuropathol Commun*. 2023;11:31.

51. Bulten W, Pinckaers H, van Boven H, et al. Automated deep-learning system for Gleason grading of prostate cancer using biopsies: a diagnostic study. *Lancet Oncol*. 2020;21:233-241.

52. Allsbrook WC, Mangold KA, Johnson MH, et al. Interobserver reproducibility of Gleason grading of prostatic carcinoma: general pathologists. *Hum Pathol*. 2001;32:81-88.

53. Jack CR, Therneau TM, Weigand SD, et al. Prevalence of biologically vs clinically defined alzheimer spectrum entities using the National Institute on Aging-Alzheimer's Association Research Framework. *JAMA Neurol*. 2019;76:1174-1183.

54. Müller-Schmitz K, Krasavina-Loka N, Yardimci T, et al. Normal pressure hydrocephalus associated with Alzheimer's disease. *Ann Neurol*. 2020;88:703-711.

55. Espay AJ, Da Prat GA, Dwivedi AK, et al. Deconstructing normal pressure hydrocephalus: ventriculomegaly as early sign of neurodegeneration. *Ann Neurol*. 2017;82:503-513.

56. Kambara A, Kajimoto Y, Yagi R, et al. Long-term prognosis of cognitive function in patients with idiopathic normal pressure hydrocephalus after shunt surgery. *Front Aging Neurosci*. 2020;12: 617150.

57. Elobeid A, Laurell K, Cesarini KG, et al. Correlations between mini-mental state examination score, cerebrospinal fluid biomarkers, and pathology observed in brain biopsies of patients with normal-pressure hydrocephalus. *J Neuropathol Exp Neurol*. 2015; 74:470-479.

58. Seppala TT, Nerg O, Koivisto AM, et al. CSF biomarkers for Alzheimer disease correlate with cortical brain biopsy findings. *Neurology*. 2012;78:1568-1575.

59. Graff-Radford NR. Alzheimer CSF biomarkers may be misleading in normal-pressure hydrocephalus. *Neurology*. 2014;83: 1573-1575.

60. Vanninen A, Nakajima M, Miyajima M, et al. Elevated CSF LRG and decreased Alzheimer's disease biomarkers in idiopathic normal pressure hydrocephalus. *J Clin Med*. 2021;10:1-10.

61. Libard S, Alafuzoff I. Alzheimer's disease neuropathological change and loss of matrix/neuropil in patients with idiopathic normal pressure hydrocephalus, a model of Alzheimer's disease. *Acta Neuropathol Commun*. 2019;7:98.

62. Pomeraniec IJ, Bond AE, Lopes MB, et al. Concurrent Alzheimer's pathology in patients with clinical normal pressure hydrocephalus: correlation of high-volume lumbar puncture results, cortical brain biopsies, and outcomes. *J Neurosurg*. 2016;124:382-388.